J Appl Electrochem (2010) 40:749–755
DOI 10.1007/s10800-009-0053-6

ORIGINAL PAPER

Residential electrical power storage scenario simulations with a large-scale lithium ion battery

K. Darcovich · N. Gupta · I. J. Davidson · T. Caroni

Received: 19 May 2009 / Accepted: 1 December 2009 / Published online: 19 December 2009

Abstract The advent of time-of-use (TOU) household electricity prices provides an opportunity for large lithium ion batteries to become a component of residential electrical power equipment for either storage or cogeneration. This project investigates household power use and cogeneration scenarios combined with lithium ion battery technology via simulation. The simulation treats transient battery charge and discharge based on electrochemical fundamentals. The analysis of both storage and cogeneration systems containing a batteries serves to demonstrate economic advantages of these types of power storage, as well as to identify size, materials, and performance criteria suitable for designing a lithium ion battery unit meeting real application demands.

Keywords Transport modeling · Lithium ion battery · Coupled simulation · Residential cogeneration

1 Introduction

In order to simulate the transient discharge or charge behavior of a battery, the relevant processes must be considered on a microstructural level. A lithium ion battery consists of discrete dispersed solid phases in both the anode and the cathode regions where lithium intercalates, and a continuous electrolyte phase through the entire cell through which lithium ions diffuse.

During discharge or charge, an interphase lithium ion flux can be calculated based on the state of charge, which in turn drives a lithium ion diffusion, regulated by electric potential fields distributed spatially in the solid and electrolyte phases. The simulation of the physics described above was implemented with the open-source software, OpenFOAM. A full-field solution requires four highly coupled partial differential equations, driven by the interphase lithium ion flux. The lithium ion concentration and the electrical potential in the electrolyte phase are solved over the entire battery, the solid phase potentials must be solved in different anode and cathode sub-domains, and the solid phase lithium ion concentration is solved on individual pseudo-domains, representing the interior of spherical particles distributed spatially in the anode and cathode regions of the battery.

In order to provide some context for the study, lithium ion batteries at ratings around a 2 kW/6 kWh level are expected to play a role for residential power supply and storage. It is envisioned that they can provide some economic benefit under time-of-use pricing structures, storing energy can reduce peak power demands as well as offset costly infrastructure upgrades to electrical power grid networks. By simulating lithium ion battery physics, the aim is to help identify microstructural properties and materials which can show good responses to imposed practical current loads, or conversely demonstrate a parameter set as a target for accompanying material development research to satisfy realistic operating requirements.

The physical formulation as outlined above will be presented along with practical how-to learned in developing and implementing the model, as well as the latest simulation results obtained.

NRCC No. 51927.

K. Darcovich (✉) · N. Gupta · I. J. Davidson · T. Caroni
National Research Council of Canada, Institute for Chemical Process and Environmental Technology, Ottawa, ON K1A 0R6, Canada
e-mail: ken.darcovich@nrc-cnrc.gc.ca

T. Caroni
ICAM-Lille, 6, rue Auber, 59000 Lille, France

The case developed here has its foundation in theory developed by Newman and Tiedemann [1], and subsequent numerical models [2, 3].

2 Model formulation

A lithium ion battery delivers current via chemical reactions which occur at the electrode interfaces, driven by a difference in chemical potential. In the anode, lithium ions are released from the solid phase and diffuse through an immobile plasticized electrolyte phase to the cathode region where they are intercalated with a lithium salt. Accompanying the ionic dissociation are electrons, which constitute the electric current.

The present simulation considers the following two charge-transfer reactions,

$$\text{in the anode:} \quad \mathrm{LiC_6} \underset{k_{\text{charge}}}{\overset{k_{\text{discharge}}}{\rightleftarrows}} \mathrm{Li_{1-x}C_6} + x\mathrm{Li^+} + x\mathrm{e^-}$$

$$\text{in the cathode:} \quad \mathrm{Li_{1-x}Mn_2O_4} + x\mathrm{Li^+} + x\mathrm{e^-} \underset{k_{\text{charge}}}{\overset{k_{\text{discharge}}}{\rightleftarrows}} \mathrm{LiMn_2O_4}$$

The kinetics of the reactions shown above are described by the Butler–Volmer equation. The derivation of the Butler–Volmer equation is given in detail in [4], and its application to the present case is further outlined in [3]. The lithium ions reside in solid particulates in each of the electrode regions. They make use of an electrolyte phase which envelopes these particulates (and also comprises a separator region) for diffusing from the anode side to the cathode side of the battery. The difference in electrical potential between the solid phases in the two electrode regions and the local electrolyte potential drives an interphase ion flux j_{loc} defined below in Eq. 5. Further, the lithium ion concentration varies radially inside the solid particulates as interphase mass transfer occurs.

A diagram of a simplified lithium ion battery configuration is shown in Fig. 1, in which a 100 cell one-dimensional grid was made for the numerical model as described below.

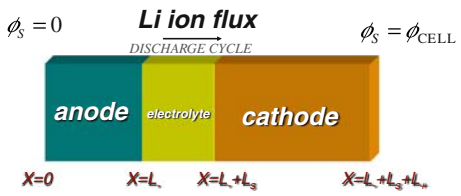

Fig. 1 One-dimensional configuration of the lithium ion battery for the numerical simulation (For improved interpretation of the color features of this figure, the reader is referred to the web version of the article)

The system considered numerically was a coupled set of equations outlined as follows.

The electrical potential in the solid phase, ϕ_{S},

$$\nabla \cdot (-\kappa_{\text{S}} \nabla \phi_{\text{S}}) = -S_{\text{a}} j_{\text{loc}} \tag{1}$$

$$\text{anode boundary conditions:} \quad \frac{\partial \phi_{\text{S}}}{\partial x} = \frac{-I_{\text{app}}}{\sigma_{\text{S}}} \text{ at } x = 0 \quad \text{and} \quad \frac{\partial \phi_{\text{S}}}{\partial x} = 0 \text{ at } x = L_-$$

$$\text{cathode boundary conditions:} \quad \frac{\partial \phi_{\text{S}}}{\partial x} = 0 \text{ at } x = L_- + L_S \quad \text{and} \quad \frac{\partial \phi_{\text{S}}}{\partial x} = \frac{-I_{\text{app}}}{\sigma_{\text{S}}} \text{ at } x = L_- + L_S + L_+.$$

An additional condition was to set $\phi_{\text{S}} = 0$ at $x = 0$ as a reference value, thus enabling the determination of the cell potential as the difference between the ϕ_{S} values at the two battery terminals.

The electrical potential in the electrolyte phase ϕ_{E}

$$\nabla \cdot \left(\kappa_{\text{E}}^{\text{eff}} \left[-\nabla \phi_{\text{E}} + \frac{2RT}{F} \left(1 + \frac{\partial \ln f}{\partial \ln c_{\text{E}}} \right) (1 - t_+) \frac{1}{c_{\text{E}}} \nabla c_{\text{E}} \right] \right) = S_{\text{a}} j_{\text{loc}} \tag{2}$$

$$\text{boundary conditions:} \quad \frac{\partial \phi_{\text{E}}}{\partial x} = 0 \text{ at } x = 0 \quad \text{and} \quad \frac{\partial \phi_{\text{E}}}{\partial x} = 0 \text{ at } x = L_- + L_S + L_+.$$

The lithium ion concentration in the electrolyte phase c_{E}

$$\epsilon \frac{\partial c_{\text{E}}}{\partial t} + \nabla \cdot \left(-D_{\text{E}}^{\text{eff}} \nabla c_{\text{E}} \right) = -\frac{S_{\text{a}} j_{\text{loc}} (1 - t_+)}{F} \tag{3}$$

$$\text{boundary conditions:} \quad \frac{\partial c_{\text{E}}}{\partial x} = 0 \text{ at } x = 0 \quad \text{and} \quad \frac{\partial c_{\text{E}}}{\partial x} = 0 \text{ at } x = L_- + L_S + L_+.$$

The lithium ion concentration in the solid phases c_{S} solved on a separate pseudo-domain over the internal radius of the solid particle, assumed to be spherical.

$$\frac{\partial c_{\text{S}}}{\partial t} + \frac{1}{r^2} \frac{\partial}{\partial r} \left(-r^2 D_{\text{S}} \frac{\partial c_{\text{S}}}{\partial r} \right) = 0 \tag{4}$$

$$\text{boundary conditions:} \quad \frac{\partial c_{\text{S}}}{\partial r} = 0 \text{ at } r = 0 \quad \text{and} \quad \frac{\partial c_{\text{S}}}{\partial r} = \frac{-j_{\text{loc}}}{D_{\text{S}}} \text{ at } r = R.$$

The interphase ion lithium ion flux j_{loc}

$$j_{\text{loc}} = i_0 \left(\exp\left(\frac{\eta F}{RT} \right) - \exp\left(\frac{-\eta F}{RT} \right) \right) \tag{5}$$

In Eq. 5, $\eta = \phi_{\text{S}} - \phi_{\text{E}} - \phi_{\text{ref}}(c_{\text{S,surf}})$, and the term $i_0 = k_0 \sqrt{c_{\text{E}} (c_{\text{S,max}} - c_{\text{S,surf}}) c_{\text{S,surf}}}$. The value $\phi_{\text{ref}}(c_{\text{S,surf}})$ is an

equilibrium reference potential, determined at the solid phase material at the state of charge corresponding to the surface lithium ion concentration. Values for $c_{S,max}$, the maximum solid phase ion concentrations are from Table II of reference [3]. The applied current density I_{app} is set at a constant value, representing the imposed load on the battery. It is partitioned through the two phases, so that,

$$I_{app} = i_E + i_S. \quad (6)$$

Explicitly, by Ohm's Law, it can be stated,

$i_S = -\sigma_S \nabla \phi_S$ and, the relation between current and potential in the electrolyte phase is,

$$i_E = -\kappa_E^{eff} \nabla \phi_E + \frac{\kappa_E^{eff} RT}{F}\left(1 + \frac{\partial \ln f}{\partial \ln c_E}\right)(1 - t_+)\frac{1}{c_E}\nabla c_E$$

The current transfer at the terminals occurs entirely via the solid phase, such that at $i_S = I_{app}$ at $x = 0$ and $x = L_- + L_S + L_+$, and $i_E = I_{app}$ at $x = L_-$ and $x = L_- + L_S$.

3 System parameters

As mentioned above, the battery is modeled with properties from LiC_6 and $LiMn_2O_4$ solid particles in the anode and cathode regions, respectively. The electrolyte phase is taken as 2:1 v/v mixture of ethylene carbonate and dimethyl carbonate [3]. Material morphological parameters, expressions for conductivity, diffusion constants, material properties, open circuit potentials, and reaction kinetic constants are given in [2, 3]. The battery modeled a small coin cell type device with an anode thickness of 100 μm, a separator thickness of 52 μm, and a cathode thickness of 174 μm. A constant temperature of 25 °C was assumed. For the initial test, the applied current was taken as 1.75 A m^{-2}.

4 Numerical implementation

The model described above was implemented numerically with the open-source software OpenFOAM (Field Operation And Manipulation), which is an object-oriented high level code designed for treating problems which can be represented by partial differential field equations [5]. Of interest in this particular case was that the system of four partial differential equations was highly coupled, and it required sub-domain solutions on the anode and cathode regions to accommodate internal boundary conditions, as well as a pseudo-domain solution for internal lithium ion concentration profiles in particulates considered to be dispersed in the electrolyte phase.

Table 1 Time-of-use pricing scheme for the province of Ontario, Canada, as of November 1, 2007 [10]

Time (h)	TOU Period	¢ (kWh)
07–11	On-peak	8.7
11–17	Mid-peak	7.0
17–22	On-peak	8.7
22–07	Off-peak	3.0

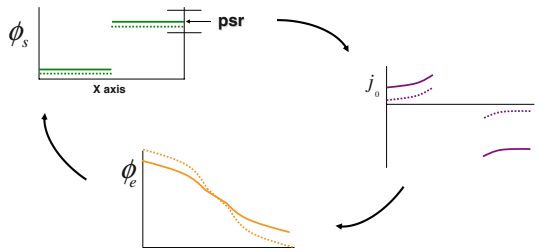

Fig. 2 Iteration on ϕ_S, indicated as guess value psr, is implemented to update j_{loc} in a loop to obtain the right solution for the imposed current density, I_{app}

Iteration control had to be handled in a more deliberate manner to maintain numerical stability. OpenFOAM is designed to solve sequentially each equation to a small residual. This is not desirable with a highly coupled system of many equations. Further, the system was non-linear, requiring a Newton–Rhapson type iteration to seek out a value of the solid phase electrical potential at the cathode terminal, as Eq. 2 is free floating with two gradient boundary conditions, and requires a reference value to allow the system of equations to converge. The check on the correct reference value for ϕ_S is made knowing that $i_S = I_{app}$ at the cathode terminal, and the iterative method to arrive at a consistent value for the system is shown in Fig. 2.

Time steps of 0.1 s were chosen. For each time step, the solution for the set of ϕ_S, ϕ_E, and j_{loc} was arrived at iteratively solving each equation no more than five times in a row to conserve numerical stability. This part of the solution was based on the battery state of charge, and determined a rate value (j_{loc}, mol m^{-2} s^{-1}) which was then used to solve the temporal equations for c_E and c_S.

5 Results and discussion

A test case for a discharge cycle of 2,000 s was run. The highly sensitive interphase lithium ion flux profiles were found to match results from a preliminary calculation done with COMSOL Multiphysics reproducing work by Doyle [6, 7] as a benchmark exercise. Cell potential and j_{loc} profiles at various times are shown in Fig. 3. The cell potential is defined as the difference between the solid phase potentials of the two battery terminals, essentially ϕ_S at the cathode terminal, since the anode value was set to zero. An improved interpolation function (at low SOC values) for the $LiMn_2O_4$ reference potential versus state of

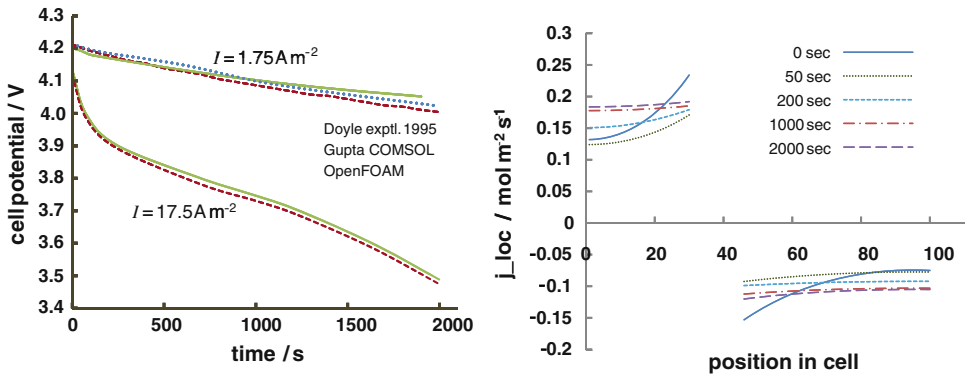

Fig. 3 The curve on the *left* shows cell potential over a 2,000 s discharge at current densities of 1.75 and 17.5 A m^{-2}. Simulation data are compared to experimental data from Doyle [6]. The plot on the *right* shows spatial profiles of j_{loc} as a function of spatial position

charge was used in the present study as compared to the COMSOL study, accounting for much of the observed difference in the cell potential at the lower discharge rate of 1.75 A m^{-2}. Experimental data from Doyle [6] are also given in Fig. 3. For the higher discharge rate of 17.5 A m^{-2}, the maximum cell voltage drops more quickly to the plateau range on the state of charge curve [2], and the discharge curves are far more similar.

Figure 4 shows ϕ_E values for different times during the discharge cycle. The trends match expected behavior. It should be noted that there is not a direct monotonic behavior here, since the electrolyte potential is a complex interdependent function of other system variables whose patterns can be somewhat oscillatory as the main cell potential drops over the course of the battery discharge.

The lithium ion concentration profiles in the electrolyte and solid phases are shown in Fig. 5. The lithium diffuses out of the solid phase in the anode, then through the separator region and reasssociates in the cathode region. Thus, the ion concentration in the electrolyte phase increases in the anode region and decreases in the cathode region. These changes are compensated by opposite changes in the respective regions for the solid phase such that the system mass balance is respected. Note that the solid concentration given is at the surface of the particulates.

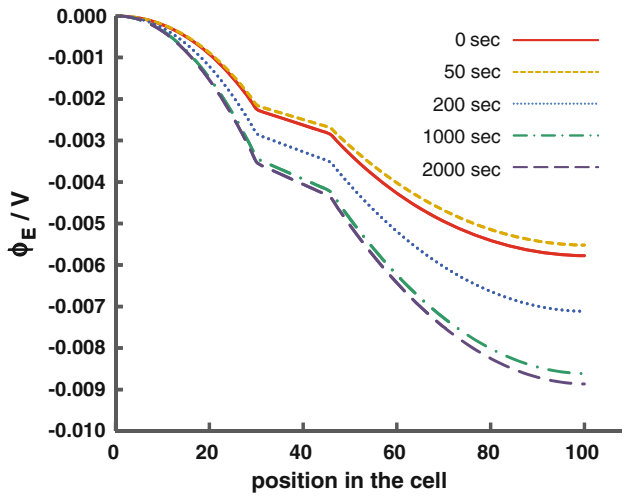

Fig. 4 Profiles of the electrolyte potential ϕ_E for various time levels

5.1 Load-leveling scenario

A digitally monitored test house is available for research purposes at the National Research Council of Canada in Ottawa. In 2002, typical electrical load profiles were measured over entire 24-h cycles, on many dates over the course of the year. The base load was taken from the summer data, and does not include any air handler, furnace, or air conditioning loads. All meter data was recorded at 5-min intervals, thus peaks in the load profile are averaged over a 5-min period [8].

It was desired to investigate the role of a large size lithium ion battery for delivering peak demand power to a residence. A notional battery size and power for this application would be about 2 kW/6 kWh. At present, commercial batteries exist at 3.8 kW/1.75 kWh ratings, therefore a bank of three such units (Valence Technology, model U27-12XP) would be suitable for the cases discussed below [9]. For reference, such batteries are block shaped, weigh about 20 kg each, and have linear dimensions of 306 × 173 × 225 mm.

In order to achieve this, a 5 m^2 lithium ion battery surface area a_S was assumed, in a series stack cell configuration, with $N = 66$ units, to maintain a minimum of 230 V, (and 3.5 V in a single cell) where the current load on the battery system is determined by:

$$I_{app} = \frac{P - P_{MIN}}{VNa_s}, \tag{7}$$

where P represents the temporal power demand above the threshold value of P_{MIN} of 3 kW for peak power assistance. Figure 6 shows power consumption measured over the course of two 24-h periods, one in the summer and other in winter. The summer power consumption is higher, attributable to air conditioning requirements, and is the basis for the analysis done here. With P_{MIN} set to 3 kW, the portions

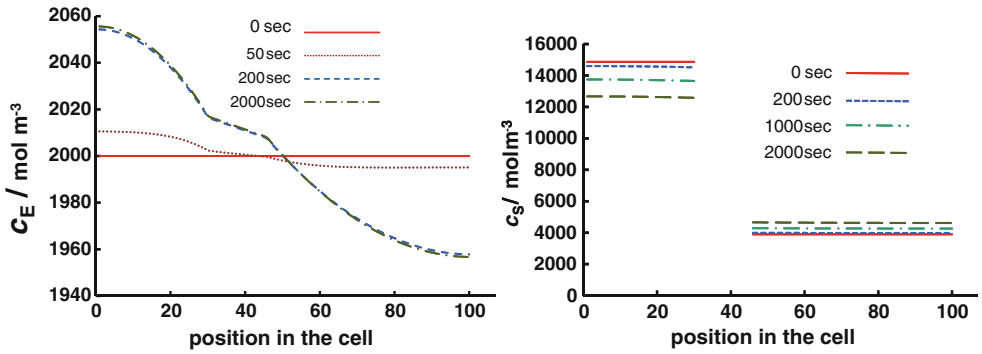

Fig. 5 Profiles of the lithium ion concentration c_E in the electrolyte phase on the *left*, and c_S in the solid phase on the *right*

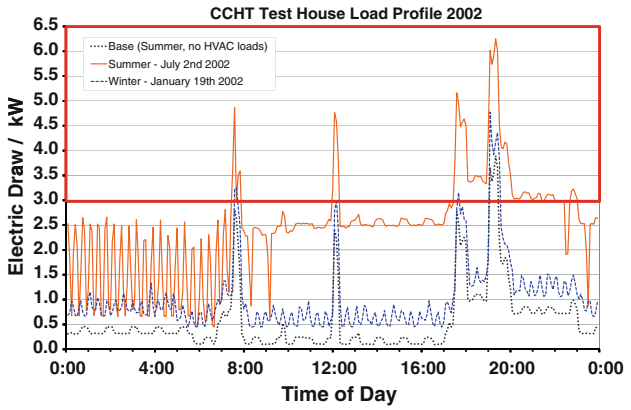

Fig. 6 Data set for Canadian residential power consumption over 24-h periods. The electrical draw requirements inside the box covering the 3.0–6.5 kW range are to be provided by a large lithium ion battery

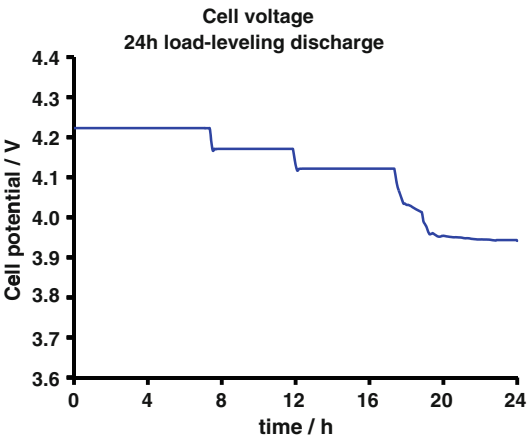

Fig. 8 Cell potential during the discharge of a large lithium ion battery for the 24-h test period

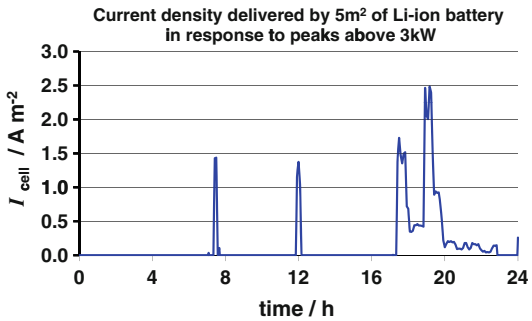

Fig. 7 Electrical load profile demanded of the large lithium ion battery for the 24-h test period

of the power demand curve enclosed in the box from 3.0 to 6.5 kW range in Fig. 6 are to be supplied by the battery. Thus, the battery simulation, as outlined above was used with a temporal load profile shown in Fig. 7, determined from Eq. 7. When the load is applied, the notional battery responded as shown in Fig. 8.

The integrity of the lithium ion battery can be maintained for thousands of charge–discharge cycles if the cell voltage is not allowed to drop below about 3.5 V. As shown in Fig. 8, the hypothetical 66 sub-unit, 5 m^2 area lithium ion battery can serve to adequately provide 24-h power demands above 3 kW under high summer use conditions. Further, the cell potential dropped to just under 4.0 V, while providing peak power for the day. The cell could be recharged in about 4 h, readily achievable during the night Off-peak period as shown in Fig. 10.

5.2 Cogeneration scenario

The advent of TOU pricing for grid-based electricity will provide a context that will encourage the use of residential power storage as a cost savings strategy. Table 1 gives TOU pricing data for Ontario, Canada, quoted in $CAD [10].

Assuming the same stack configuration as outlined in Sect. 5.1, consider running a 2 kW Stirling engine to co-generate heat and electricity. The battery will be set to discharge during On-peak pricing periods, and will charge during Mid-peak and Off-peak periods. The trial assumes

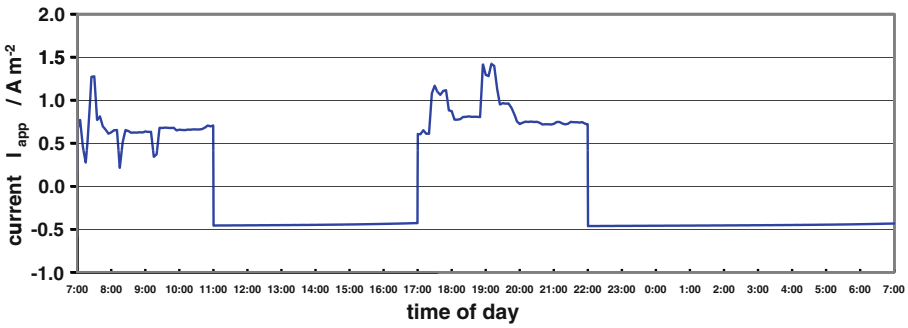

Fig. 9 Electrical load profile demanded of the large lithium ion battery for two peak pricing periods during the 24-h test cycle. The charging currents shown restore the battery to a full state of charge for the ensuing discharge periods

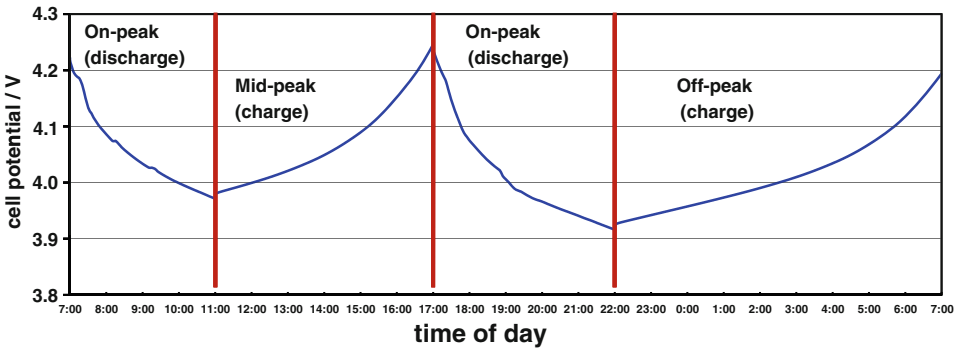

Fig. 10 Cell potential of a large lithium ion battery during the discharge and charge periods for the 24-h test cycle

30% efficiency for electrical generation (f_{eff}), and assigns the battery to cover 35% (α_1) of the morning and 30% (α_2) of the evening On-peak power demand. The current densities for charging and discharging are thus,

$$I_{\text{Discharge}} = \frac{\alpha_i P_{\text{HOUSE}}(t)}{VNa_s} \quad \text{and,} \quad I_{\text{Charge}} = \frac{(f_{\text{eff}} \cdot P)_{\text{Stirling}}}{VNa_s}. \tag{8}$$

Graphically, $I_{\text{Discharge}}$ and I_{Charge} follow the demand supply curve shown in Fig. 9. The battery is constrained by having to return to a full state of charge (cell potential around 4.2 V) at the end of the cycle. This limits the values of α_1 and α_2, the fraction of total power demand that could be supplied by the battery on a continuing basis. The cell potential over the course of the 24-h period during which two discharge and two charge periods occur, is plotted in Fig. 10.

Assuming the heat derived from the Stirling engine is economically viable, cogeneration with a lithium ion battery under the conditions outlined above can reduce daily power consumption from the electrical grid by 30% from 61 to 43 kWh, at a cost savings of $CAD440/year.

6 Conclusions

The results obtained show that a realistic simulation of the discharge of a lithium ion battery using OpenFOAM has been achieved. The simulation features two-subdomains, a pseudo-domain and a specially adapted convergence algorithm for a highly coupled system of equations. Preliminary results confirm the accuracy of simulation when compared to other existing results, and given that the physics are implemented on a fundamental level, the simulation is readily adaptable other configurations, or for considering different combinations of materials and operating conditions.

The simulation was then implemented in the study of lithium ion batteries for residential power storage applications. Making use of real household power consumption loads showed that a large size lithium ion battery with a 2 kW/6 kWh power capacity rating would be effective for both load-leveling and cogeneration applications.

References

1. Newman J, Tiedemann W (1975) AIChE J 21(1):25–41
2. Fuller TF, Doyle M, Newman J (1994) J Electrochem Soc 141(1):1–10
3. Doyle M, Newman J, Gozdz AS, Schmutz CN, Tarascon JM (1996) J Electrochem Soc 143(6):1890–1903
4. Bockris JOM, Reddy AKN, Gamboa-Aldeco M (2000) Modern electrochemistry 2A. Fundamentals of electrodics, 2nd ed. Kluwer Academic/Plenum Publishers, Dordrecht, p 1083
5. Powell AC IV, Arroyave R (2008) JOM 60(5):32–39
6. Doyle M (1995) Ph.D. Thesis, University of California, Berkeley, p 382
7. Darcovich K, Caroni T (2008) In: Proc. 5th NRC Symposium on Computational Fluid Dynamics and Multi-scale Modeling, Ottawa, January 21, p 6

8. Bell M, Swinton M, Entchev E, Gusdorf J, Kalbfleisch W, Marchand R, Szadkowski F (2003) Development of Micro Combined Heat and Power Technology Assessment Capability at the Canadian Centre for Housing Technology, Technical Report B-6010, Canadian Centre for Housing Technology, Ottawa, December, p 48
9. Huanga H, Faulkner T, Barkera J, Saidia MY (2009). J Power Sources 189(1):748–751
10. Strapp J, King C (2007) Talbott S Ontario Energy Board Smart Price Pilot final report, Ontario Energy Board, Toronto, p 221